Surface Crack Growth Path and Fatigue Life Prediction Due to Repeated Rolling/Sliding Contact*

Takahito GOSHIMA**, Sotomi ISHIHARA**,
Masayoshi SHIMIZU**, Hirokazu YOSHIDA***
and Yuji TSUCHIDA****

This paper deals with the surface crack growth path description and the fatigue life prediction due to repeated rolling/sliding contact on the elastic half-space, accompanied by frictional heat generation and crack-face pressure. The stress intensity factors are analyzed for the surface crack which is kinked in multiple times from the inclined initial main crack. The rolling/sliding contact is simulated as a Hertzian contact pressure and a frictional load with heat generation, moving with constant velocity over the surface of the half-space. Applying the maximum energy release rate criterion to each kinked angle, the crack growth path can be described, and employing a mixed mode fatigue crack growth law, the associated fatigue life also can be predicted. The effects of frictional coefficient, slide/roll ratio and crack-face pressure on the crack growth path and associated life are considered for a high carbon-chromium bearing steel (AISI52100).

Key Words: Elasticity, Thermal Stresses, Contact Problem, Stress Intensity Factor, Crack Growth, Crack Path, Frictional Heating, Fatigue Life

1. Introduction

In gears, bearings, rollers and rails etc., an initial crack may be propagated into the tribological failure, such as pitting, spalling or shelling etc., due to rolling contact. Since the experimental investigation of Way[1] who concluded that the pit formation was the result of surface crack propagation caused by lubricant seepage into the crack, the mechanism involved with rolling contact fatigue failure has been a topic of interest to many investigators. For example, as comparative recent experimental investigations of contact fatigue surface pitting, Zhou[2] made careful observations of surface pit formation by using a two-disc machine, and studied crack initiation as well as propagation in detail. Kaneta et al.[3], observed branched cracks under repeated water lubricated rolling-sliding contact. The first attempt of fracture mechanics for surface pitting failure was carried out by Keer et al.[4] They studied surface fatigue crack propagation including the effects of fluid pressure and crack face friction, although in an approximate manner, and examined these effects on fatigue life. They postulated that crack propagation is driven by the cyclic shear mode. Following their work, considerable research for rolling contact from fracture mechanics viewpoint has been reported. Bower[5] has been able to combine the effects of shear along with the fluid entrapment mechanism. Crack face friction was incorporated in an exact manner, appropriate with the Coulomb friction model. The effects of fluid entrapment and sliding-locking of the crack faces on Mode I and Mode II stress intensity factors were studied. Murakami et al.[6] and Kaneta et al.[7] have applied three-dimensional fracture mechanics to study contact fatigue surface pitting. They postulated in experimental and fracture mechanics viewpoint that the lubricant con-

* Received 2nd June, 2003 (No. 02-0029). Japanese original: Trans. Jpn. Soc. Mech. Eng., Vol. 68, No. 672, A (2002), pp. 1198-1205 (Received 11th January, 2002)

** Faculty of Engineering, Toyama University, 3190 Gofuku, Toyama city, Toyama 930-8555, Japan. E-mail: goshima@eng.toyama-u.ac.jp

*** Jamco Corporation, 6-11-25 Oosawa, Mitaka city, Tokyo 181-0015, Japan

**** Anden Corporation, 3 Iyama, Shinome, Anjyou city, Aichi 446-0073, Japan

tribute to the pitting formation. Moreover, Goshima et al.[8]–[10] have studied a series of analysis for the thermal stress intensity factors due to rolling contacts with frictional heat.

The above research has considered only straight growth of cracks. However, the actual crack is apt to branch in the direction approximately perpendicular to the maximum tensile stress and is propagated into a pitting failure. As to the analysis for branched crack due to the rolling contact, Farris, et al.[11], Yu, et al.[12] and Mukai, et al.[13] have studied the kinked direction from a subsurface crack. However, their results are not apply to the surface crack., and they do not consider the crack growth path. In order to gain a better understanding for the mechanism of the surface tribological failure, the prediction of surface crack growth path and fatigue life due to the rolling contact with thermal stresses must be considered.

In this study, we analyzed the stress intensity factors for a multiple kinked crack applied hydraulic internal pressure in a half-space due to rolling contact with frictional heat. On the basis of the results of stress intensity factors for the multiply kinked crack model, and applying the maximum energy release rate criterion[14] to each kinks in order, the two-dimensional fatigue crack growth path are simulated, and making use of the fatigue crack growth law[15] for a high carbon chromium bearing steel (AISI52100), the propagation fatigue lives are predicted. And the thermomechanical effects such as the frictional coefficient, sliding/rolling ratio and the crack-face fluid pressure on the fatigue crack propagation life and induced fatigue pitting failures are considered.

2. Problem Formulation

An elastic half-space containing a multiple kinked crack ($\tilde{l}_1, \tilde{l}_2, \cdots, \tilde{l}_n$) is subjected to rolling-sliding contact accompanied by frictional heat with constant velocity V, as shown as Fig. 1. The coordinates ($\tilde{x}$, $\tilde{y}$) (which move with constant rolling velocity V) are fixed to the roller. The coordinates, ($\tilde{\xi}_k$, $\tilde{\zeta}_k$); ($k=1, 2, \cdots, n$) are fixed each branched cracks. In the analysis, the dimensionless parameters for the branched crack k (where $k=1, 2, \cdots, n$), and are shown as follows.

$(x, y)=(\tilde{x}/c, \tilde{y}/c)$, $(\xi_k, \zeta_k)=(\tilde{\xi}_k/c, \tilde{\zeta}_k/c)$,
$l_k=\tilde{l}_k/c$,
$x_k=\tilde{x}_k/c$, $S_r=V_s/V$, $P_e=cV/\kappa_t$, $\beta_k^*=180°-\beta_k$,
$H_0=2\alpha_0 G_0 \kappa_t(1+\nu)/\{K_t(1-\nu)\}$, $P(x)=P_1(\tilde{x})/P_0$

Where, c is half contact length, κ_t is thermal diffusivity, K_t is thermal conductivity, G_0 is shear modulus, ν is Poissoin's ratio, α_0 is coefficient of thermal expansion, P_0 is the maximum contact pressure, V_s is the sliding velocity during rolling contact,

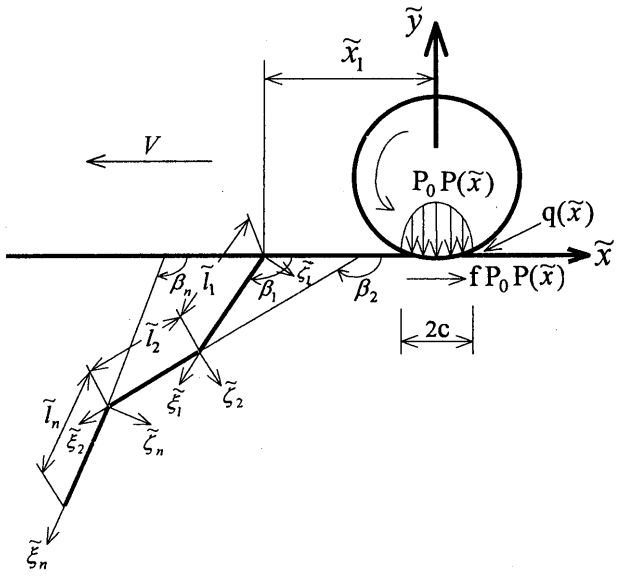

Fig. 1 Geometry and coordinate system

P_e is Peclet number, S_r is slide-roll ratio. Then, the frictional heat generation $Q_1(\tilde{x})$ is given as follows:

$$Q_1(\tilde{x})=fV_sP_1(\tilde{x})=fV_sP_0P(x)=fVS_rP_0P(x) \quad (1)$$

The region outside the area of contact is assumed to be thermally insulated. Furthermore, it is assumed that the temperature distribution $T(x, y)$ is not affected by the presence of cracks. Thus, the thermal boundary conditions can be given as follows.

$$\left(\frac{\partial T}{\partial y}\right)_{y=0}=\begin{cases} fcVS_rP_0P(x)/K_t, & |x|<1 \\ 0, & |x|>1 \end{cases} \quad (2)$$

$$(T)_{y\to-\infty}=0 \quad (3)$$

The mechanical boundary conditions on the surface and at infinity of the half-space are given as

$$(\sigma_{yy})_{y=0}=\begin{cases} -P_0P(x) & |x|\le 1 \\ 0 & |x|>1 \end{cases} \quad (4)$$

$$(\sigma_{xy})_{y=0}=\begin{cases} fP_0P(x) & |x|\le 1 \\ 0 & |x|>1 \end{cases} \quad (5)$$

$$(\sigma_{pq})y_{=-\infty}=0 \quad (p, q=x, y) \quad (6)$$

Assuming that crack face friction is neglected, the boundary condition along the kth kinked cracks may be expressed as:

$$(\sigma_{\xi_k\zeta_k})_{\zeta_k=0}=0 \quad 0<\xi_k<l_k \quad (k=1, 2, \cdots, n) \quad (7)$$

$$(\sigma_{\zeta_k\zeta_k})_{\zeta_k=0}=\begin{cases} -P_2(x, \xi_k) & |x|\le 1 \\ 0 & |x|>1 \end{cases} \quad \xi_k\in\xi_k^{op}$$
$$(k=1, 2, \cdots, n) \quad (8)$$

where ξ_k^{op} is the crack face opening region of the kth kinkeded crack, and $P_2(x, \xi_k)$ is the fluid pressure applied at the crack face, which is taken either as an uniform distribution pressure or no pressure as:

$$P_2(x, \xi_k)=\begin{cases} 0 & : \textit{no pressure} \\ P_0P(x) & : \textit{uniform pressure} \end{cases} \quad (9)$$

3. Stress Analysis

The stress field σ_{pq} is represented by superposi-

tion as:

$$\sigma_{pq}=\sigma^0_{pq}+\sigma^1_{pq},\ (p,\ q=x,\ y \text{ or } \xi_k,\ \zeta_k) \tag{10}$$

Here, σ^0_{pq} denotes the stress in an uncracked half-space subjected to the rolling-sliding contact loading and heat generation in the contact region. The stresses σ^1_{pq} denotes the stress disturbance induced by the crack.

The solution of the stress σ^0_{pq} which satisfies the boundary conditions Eqs.(2) - (6) is represented as follows[9].

$$\frac{\sigma^0_{pq}}{P_0}=\begin{cases}\displaystyle\int_{-1}^{1}P(t)F_{pq}dt, & x\le -1\\ \displaystyle\int_{-1}^{x}P(t)G_{pq}dt+\int_{-1}^{1}P(t)F_{pq}dt, & -1<x\le 1\\ \displaystyle\int_{-1}^{1}P(t)G_{pq}dt+\int_{-1}^{1}P(t)F_{pq}dt, & x>1\end{cases} \tag{11}$$

where,

$$F_{pq}=H_0fS_rA_{pq}(2\pi P_e)^{-0.5}\{(x-t)^2+y^2\}^{-0.75}+\{y+(2H_0S_r-1)(x-t)f\}B_{pq}\{(x-t)^2+y^2\}^{-2}/\pi \tag{12}$$

$$G_{ij}=0.5fS_rD_{ij}(\pi P_e)^{-0.5}(x-t)^{-2.5}e^{-Py^2/4(x-t)} \tag{13}$$

$A_{xx}=\cos\theta_1+\sin\theta_1-1.5\cos\theta_0(\cos\theta_2+\sin\theta_2)$

$A_{yy}=\cos\theta_1+\sin\theta_1+1.5\cos\theta_0(\cos\theta_2+\sin\theta_2)$

$A_{xy}=1.5\cos\theta_0(\cos\theta_2-\sin\theta_2)$

$\theta_0=\tan^{-1}\{(x-t)/y\},\ \theta_1=1.5\theta_0,\ \theta_2=2.5\theta_0$

$B_{xx}=(x-t)^2,\ B_{yy}=y^2,\ B_{xy}=-y(x-t)$

$D_{xx}=P_ey^2-2(x-t)-4P_e(x-t)^2$

$D_{yy}=2(x-t)-P_ey^2,\ D_{xy}=2y(x-t)P_e$

To account for the stresses caused by the crack, we consider the problem of a discrete dislocation α_j present at the point $z=z_{0j}(\xi_j=\eta_j)$ on the jth branched crack in an infinite space. Then the dislocation density is defined as:

$$\alpha_j=\frac{G_0}{i\pi c(\kappa+1)}\{[U_{\xi_j\xi_j}]+i[U_{\zeta_j\zeta_j}]\}e^{-i\beta_j},\quad (j=1,2,\cdots,n) \tag{14}$$

where $\{[U_{\xi_j\xi_j}]+i[U_{\zeta_j\zeta_j}]\}$ represent the displacement jumps, and z_{0j} is represented as follows.

$$z_{0j}=\begin{cases}\eta_1e^{-i\beta_1}+x_1, & (j=1)\\ \eta_je^{-i\beta_j}+\displaystyle\sum_{m=1}^{j-1}l_me^{-i\beta m}, & (j=2,3,\cdots,n)\end{cases} \tag{15}$$

The solution to this problem is solved using the following complex potential functions[16].

$$\Phi_2(z)=\frac{\alpha_j}{z-z_{0j}} \tag{16}$$

$$\Psi_2(z)=\frac{\overline{\alpha_j}}{z-z_{0j}}+\frac{\alpha_j\,\overline{z_{0j}}}{(z-z_{0j})^2} \tag{17}$$

Then the stress representation is given by Muskhelishvili[17] as:

$$(\sigma^d_{\zeta_j\zeta_j}-i\sigma^d_{\xi_j\zeta_j})_{\Phi_2,\Psi_2}=\Phi_2(z)+\overline{\Phi_2(z)}+\{z\overline{\Phi_2'(z)}+\overline{\Psi_2(z)}\}e^{2i\beta_j} \tag{18}$$

where primes denote differentiation with respect to z. An additional potential Φ_3, which is required to remove the surface tractions, is conveniently written in terms of Φ_2, Ψ_2[17].

$$\Phi_3(z)=\begin{cases}-\overline{\Phi_2}(z)-z\overline{\Phi'}(z)-\overline{\Psi_2}(z), & \mathrm{Im}(z)<0\\ \Phi_2(z), & \mathrm{Im}(z)>0\end{cases} \tag{19}$$

Then the stress representation is represented as[17]:

$$(\sigma^d_{\zeta_j\zeta_j}-i\sigma^d_{\xi_j\zeta_j})_{\Phi_3}=\Phi_3(z)+\overline{\Phi_3(z)}-\{\overline{\Phi_3(z)}+\Phi_3(\bar z)-(z-\bar z)\overline{\Phi_3'(z)}\}e^{2i\beta_j} \tag{20}$$

Superposing Eqs.(18) and (20), the stress field due to a discrete edge dislocation α_j in a half space is represented in coordinates $(\xi_j,\ \zeta_j)$ as:

$$\sigma^d_{\zeta_j\zeta_j}-i\sigma^d_{\xi_j\zeta_j}=(\sigma^d_{\zeta_j\zeta_j}-i\sigma^d_{\xi_j\zeta_j})_{\Phi_2,\Psi_2}+(\sigma^d_{\zeta_j\zeta_j}-i\sigma^d_{\xi_j\zeta_j})_{\Phi_3} \tag{21}$$

Replacing α_j by distributed dislocation density defined along the each branched cracks $(j=1,2,\cdots,n)$, the stress σ^1_{pq} can be obtained by using Eq.(21) as a Green's function.

$$\sigma^1_{\zeta_k\zeta_k}-i\sigma^1_{\xi_k\zeta_k}=\sum_{j=1}^{n}\left\{\int_0^{l_j}(\sigma^d_{\zeta_j\zeta_j}-i\sigma^d_{\xi_j\zeta_j})d\eta_j\right\} \tag{22}$$

Superposing Eqs.(22) and (11) as Eq.(10), the stress solution σ_{pq} which satisfy the boundary conditions Eqs.(2) - (6). After the coordinate transformation of σ_{pq} along the each branched coordinates $(\xi_k,\ \zeta_k)$. Substituting these results the boundary conditions Eqs.(7), (8), the following singular integral equations for $\alpha_k\ (k=1,2,\cdots,n)$ are obtained.

$$2e^{i\beta_k}\int_0^{l_k}\frac{\alpha_k(\eta_k)}{\xi_k-\eta_k}d\eta_k+\sum_{j=1}^{n}\int_0^{l_k}\{\alpha_j(\eta_j)F_{1k}(\xi_k,\eta_j)+\overline{\alpha_j(\eta)}F_{2k}(\xi_k,\eta_j)\}d\eta_j=-(\sigma^0_{\zeta_k\zeta_k}-i\sigma^0_{\xi_k\zeta_k})_{\zeta_k=0}-P_2(\xi_k),\ (k=1,2,\cdots,n) \tag{23}$$

where, kernel functions $F_{1k}(\xi_k,\eta_j)$, $F_{2k}(\xi_k,\eta_j)$ are given as:

$$F_{1k}(\xi_k,\eta_j)=\hat\Phi_3(z_k,z_{0j})+(1-e^{2i\beta_k})\overline{\Phi_3^*(z_k,z_{0j})}-e^{2i\beta_k}\{\overline{\hat\Phi_3(z_k,z_{0j})}-(z_k-\overline{z_k})\overline{\Phi_3^{*\prime}(z_k,z_{0j})}\}+(1-\delta_{kj})L_{1k}(\xi_k,\eta_j) \tag{24}$$

$$F_{2k}(\xi_k,\eta_j)=\Phi_3^*(z_k,z_{0j})+\overline{\hat\Phi_3(z_k,z_{0j})}-e^{2i\beta_k}\{\overline{\hat\Phi_3(z_k,z_{0j})}+\Phi_3^*(\overline{z_k},z_{0j})-(z_k-\overline{z_k})\overline{\hat\Phi_3^{*\prime}(z_k,z_{0j})}\}+(1-\delta_{kj})L_{2k}(\xi_k,\eta_j) \tag{25}$$

$$L_{1k}(\xi_k,\eta_j)=\Phi_2^*(z_k,z_{0j})+\overline{\Phi_2^*(z_k,z_{0j})}e^{2i\beta_k}$$

$$L_{2k}(\xi_k,\eta_j)=\overline{\Phi_2^*(z_k,z_{0j})}+\{z_k\overline{\Phi_2^{*\prime}(z_k,z_{0j})}+\overline{\Psi_2^*(z_k,z_{0j})}\}e^{2i\beta_k}$$

$$\hat\Phi_3(z,z_0)=\begin{cases}-1/(z-\overline{z_0}), & \mathrm{Im}(z)<0\\ 1/(z-z_0), & \mathrm{Im}(z)>0\end{cases}$$

$$\Phi_3^*(z,z_0)=\begin{cases}(\overline{z_0}-z_0)/(z-\overline{z_0})^2, & \mathrm{Im}(z)<0\\ 0, & \mathrm{Im}(z)>0\end{cases}$$

$$\Phi_2^*(z,z_0)=1/(z-z_0),\ \Psi_2^*(z,z_0)=\overline{z_0}/(z-z_0)^2$$

$$\delta_{kj}=\begin{cases}1, & k=j\\ 0, & k\ne j\end{cases};\quad\begin{cases}z_1=\xi_1e^{-i\beta_k}+x, & k=1\\ z_k=\xi_ke^{-i\beta_k}+\displaystyle\sum_{m=2}^{k-1}l_me^{-i\beta_m}, & k=2,3,\cdots,n\end{cases}$$

4. Stress Intensity Factors and Numerical Calculations

4.1 Derivation of stress intensity factors

Equation (23) was solved numerically using the piecewise quadratic method of Gerasoulis[18]. The each dislocation densities $\alpha_k(\eta_k)$ are written with separating the singularities as

$$\alpha_k(\eta_k)=\frac{P_0\tilde{\alpha}_k(\tilde{\eta}_k)}{(1-\tilde{\eta}_k)^{1/2}}e^{-i\beta_k},\quad \tilde{\eta}_k=\frac{2\eta_k}{l_k}-1 \tag{26}$$

Let us divide the interval $-1\leq\tilde{\eta}_k\leq 1$ into $2N_k$ equal parts. We define the nodal points as $\tilde{\eta}_{k,s}$ ($s=1-2N_k+1$), and use the Lagrange interpolation formula for three nodal points in the approximation. Setting the collocation points as $\tilde{\xi}_{k,r}=\tilde{\eta}_{k,r}+1/2N_k$ ($r=1-2N_k$), Eq. (23) reduces to the simultaneous linear algebraic equation for $\tilde{\alpha}_k(\tilde{\eta}_{k,s})$. Here, ξ_k^{op} in Eq. (8) are determined iteratively the degree of crack opening for a given set of parameters. Iteration was performed under the condition of the absence of overlap of the material. as $U_{\zeta_k\zeta_k}<0$. In the present numerical examples, this method generally converged within three iterations. For the number of collocation points, a good accuracy was obtained for $N_k=10$. At that time, mode I and mode II stress intensity factors at the n-kinked crack tip are given as follows.

$$K_I^*-iK_{II}^*=\frac{K_I-iK_{II}}{P_0\sqrt{c}}=\pi\sqrt{2l_n}\,\tilde{\alpha}_n(1) \tag{27}$$

Although the maximum mode I stress intensity factor $K_{I\max}$, the maximum and minimum mode II stress intensity factors $K_{II\max}$ and $K_{II\min}$ occur at different locations, stress intensity factor range $\Delta K_I=K_{I\max}$, $\Delta K_{II}=K_{II\max}-K_{II\min}$ over a complete loading cycle are used for fatigue consideration. Especially, in the present study, as a mixed mode fatigue propagation should be considered, energy release rate ΔG (Pa·m) over a complete loading cycle is defined as follows.

$$\Delta G=\frac{1-\nu}{2G_0}\{(K_{I\max})^2+(\Delta K_{II})^2\} \tag{28}$$

4.2 Numerical calculations of stress intensity factors for a single kinked crack

As the most simple example, the stress intensity factors for a single kinked crack are considered as shown in Fig. 2. Numerical calculations are carried out for the case of $c=0.4$ mm, $P_e=100$ and $P_0=2.0$ GPa being Hertzian contact pressure distribution. The material used here is a high carbon-chromium bearing steel (AISI52100). The shear modulus and Poissoin's ratio are $G_0=113.74$ GPa and $\nu=0.3$. We define the initial crack length and inclined angle are $\tilde{l}_1$ and β_1^*, the branched crack length and angle are $\tilde{l}_2$ and β_2^*. As the dimensionless parameter H_0 in Eq. (12) is almost equal to unity for most metallic materials[19],[20], we assume $H_0=1$. As the threshold value of the high carbon chromium bearing steel is $K_{I\,th}=3.4$ MPa$\sqrt{\text{m}}$, the threshold value of energy release late is assumed as

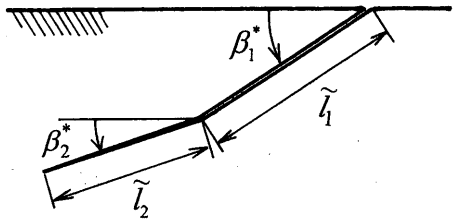

Fig. 2 Single kined crack model

$$\Delta G_{th}=(1-\nu)K_{Ith}^2/(2G_0)=50.82\ \text{Pa·m} \tag{29}$$

Actually, before the crack propagation, the crack initiation should be considered. For example, Fan, et al.[21] estimated the crack initiation life by using the Mura-Tanaka crack initiation model. However, in the present study, it is assumed that the initial crack is inclined at the angle of maximum energy release rate, and the initial crack length can be determined by the criterion of $\Delta G\cong\Delta G_{th}$. Thus, the initial crack with inclined angle $\beta_1^*=36.5°$ and crack length $\tilde{l}_1=44\ \mu$m were obtained. The branched crack length is assumed to be $\tilde{l}_2=5\ \mu$m.

Figures 3 and 4 show the effect of kinked angle β_2^* on the behavior of stress intensity factors K_I^{**}, K_{II}^* over a complete loading cycle for the case of $f=0.1$ and $S_r=0.1$. In Fig. 3, the results for no crack-face pressure are shown. When the trailing edge of the contact region is located directly at the crack, K_{II}^* attain a positive maximum $(K_{II}^*)_{\max}$, and the values of K_I^* are relatively small compared to K_{II}^*. While, in Fig. 4, the results for uniform crack-face pressure are shown. Immediately after the leading edge of the contact region passes over the crack, K_I show the maximum peak values $(K_I^*)_{\max}$ which are larger than $(K_{II}^*)_{\max}$. Comparison of the results between Figs. 3 and 4 reveals that the uniform crack-face pressure has a significant effect on the results of K_I but the uniform crack-face pressure has almost no effect on the results of K_{II}. The values of $(K_I^*)_{\max}$ and $(K_{II}^*)_{\max}$ show the maximum at $\beta_2^*=30°$ or $0°$.

In order to clarify the kinked direction, the values of $(K_I^*)_{\max}$, ΔK_{II} are shown as functions of kinked angle β_2^* in Fig. 5 ($f=0.1$) and Fig. 6 ($f=0.3$), respectively. In these figures, thermal effects are represented by the change of $S_r=0$, 0.3, 0.5, and the presence of crack-face pressure is shown with the broken line ($K_{I\max}$) or the dot-dash line (ΔK_{II}). For the case of no crack-face pressure (except $f=0.3$, $S_r=0$), mode II crack growth seems to occur in the direction of $\beta_2^*=\beta_{2\max}^{*II}$ at which ΔK_{II} takes a maximum value. For

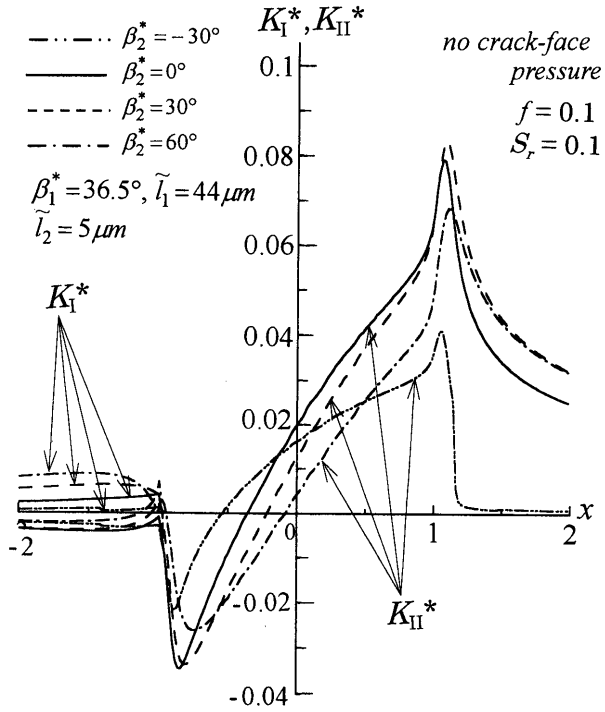

Fig. 3 Stress intensity factors K_I^* and K_{II}^* as a function of crack location for the case of no crack-face pressure

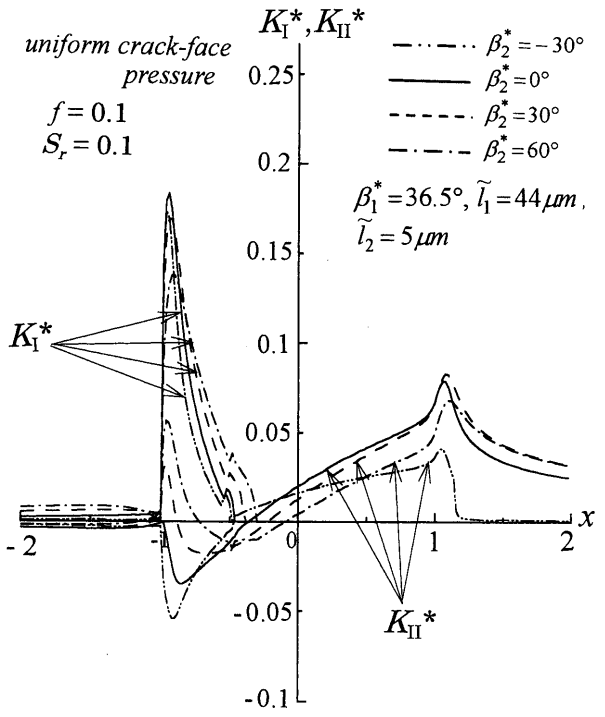

Fig. 4 Stress intensity factors K_I^* and K_{II}^* as a function of crack location for the case of uniform crack-face pressure

example, for the case of $f=0.1$ (Fig. 5), $\beta_{2\max}^{*II}=15°$ - $25°$ (for $S_r=0$ - 0.5) and for the case of $f=0.3$ (Fig. 6), $\beta_{2\max}^{*II}=25°$ - $35°$ (for $S_r=0$ - 0.5). While, for the case of uniform crack-face pressure, mixed mode

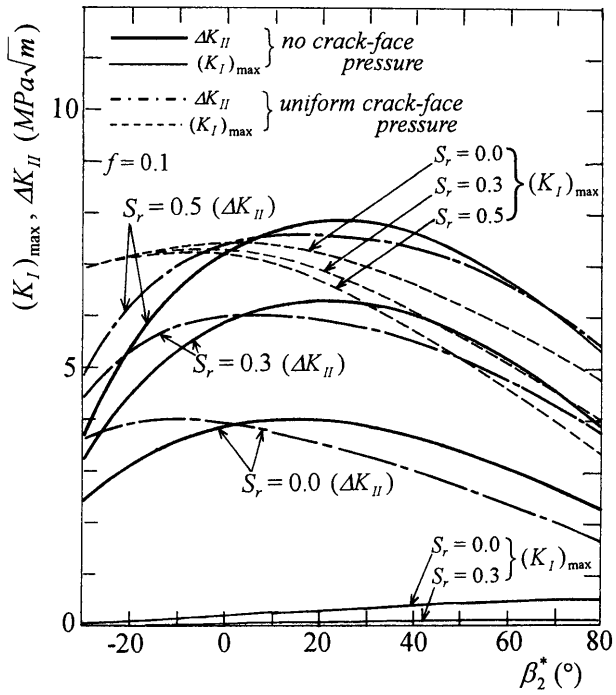

Fig. 5 $(K_I)_{max}$ and ΔK_{II} as a function of kinked angle β_2^* for the case of $f=0.1$

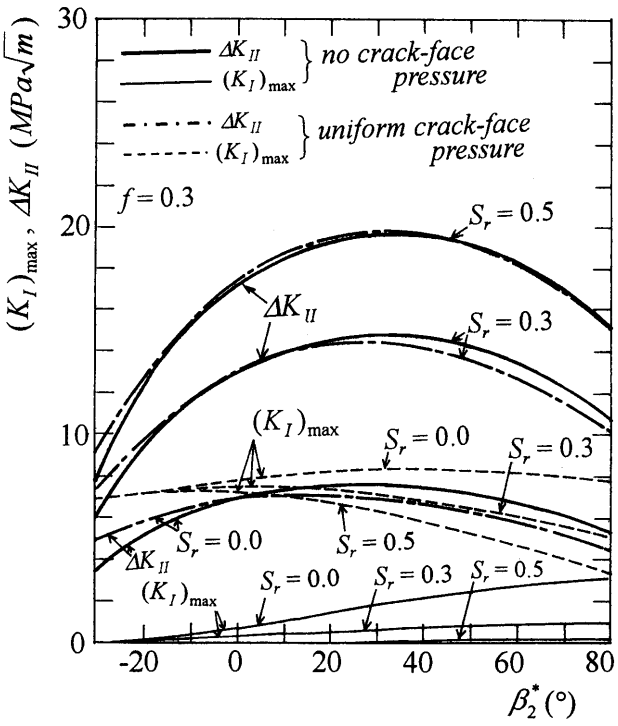

Fig. 6 $(K_I)_{max}$ and ΔK_{II} as a function of kinked angle β_2^* for the case of $f=0.3$

crack growth seems to occur in the direction $\beta_2^*=\beta_{2\max}^{*G}$ at which ΔG take a maximum value. For example, from Fig. 5 ($f=0.1$), $\beta_{2\max}^{*G}=4°$ - $3°$ for $S_r=0$ - 0.5. Thus, we can see that for the case of uniform crack-face pressure and small frictional coefficient, the crack is apt to be kinked with a steep angle.

5. Prediction of Fatigue Crack Growth Path and Life

In order to clarify the mechanism of pit formation, extending the above calculation for $n=2$ to for $n>2$, we consider the behavior of the fatigue crack growth path and fatigue life due to a repetition of the rolling contact. To account for the mixed mode propagation, the following modified Paris power low is used with Eq.(28).

$$\frac{d\tilde{l}}{dN}=\begin{cases} C_0(\sqrt{\Delta G}/\sqrt{\Delta G_{th}}^{\gamma}), & \Delta G>\Delta G_{th} \\ 0, & \Delta G>\Delta G_{th} \end{cases} \quad (30)$$

Where, $\tilde{l}$ is the total crack length, N is the cycle number, C_0, γ are the material constants, and for the case of the high carbon chromium bearing steel $C_0=2.0\times10^{-8}$m, $\gamma=4.02$ are given[15]. As mentioned above, it is assumed that the initial crack is $\tilde{l}_1=44$ μm, $\beta_1^*=36.5°$, and a crack growth increment is $\Delta\tilde{l}=\tilde{l}_k=5$ μm ($k=2, 3, \cdots, n$) in the direction of $\beta_k^*=\beta_{k\,\max}^{*G}$ at which ΔG in Eq.(28) takes a maximum value. Thus, getting the values of $\beta_{k\,\max}^{*G}$ for each steps ($k=2, 3, \cdots, n$), we can predict the crack growth path starting from the initial crack. Then, the cycle number increment ΔN_k can be obtained by using Eq.(30) : Then, we can obtain the variation of crack length $\tilde{l}=\tilde{l}_1+(n-1)\Delta\tilde{l}$ with the cycle number $N=\Delta N_2+\Delta N_3+\cdots\Delta N_n$ until n-steps (we call this relation $\tilde{l}-N$ curve).

Figure 7 displays the predicted crack growth path showing the thermal effect ($S_r=0$ - 0.5) for $f=0.1$. Then, the $\tilde{l}-N$ curve is shown in Fig. 8. From Fig. 7, for the case of no crack-face pressure, the size of the pit is given by the maximum depth : b(μm) =32, 37, 47, 60 and the width : $2a$(μm) =168, 207, 286, 359 for S_r =0, 0.1, 0.3, 0.5, respectively. Thus, an increase of the thermal effect (S_r) enlarges the size of the pitting failure, but the aspect ratio (b/a) of the pit do not change very much by S_r as b/a=0.38, 0.34, 0.33, 0.33 for S_r=0, 0.1, 0.3, 0.5, respectively. While, under uniform crack-face pressure, the initial crack is abruptly curved toward the contact surface due to the influence of tensile mode and consequently the pitting failure is reduced in size $b=26$ μm, $2a=80$ μm (b/a=0.65) for S_r=0 - 0.5. Moreover, from the $\tilde{l}$ - N curve (Fig. 8), it is evident that an increase of thermal effect (S_r) or the crack-face pressure reduces the fatigue life. Especially, when the crack-face pressure is absent, an increase of thermal effect (S_r) considerably reduce the fatigue life by an order of magnitude. For example, the fatigue life N_f decreases from a value of $N_f=6.8\times10^5$ for $S_r=0$ to a value of $N_f=8\times10^4$ for $S_r=0.5$. Moreover, the uniform crack-face pressure gives a much greater reduction in life, by an order of magnitude, as compared to no crack-face pressure. For

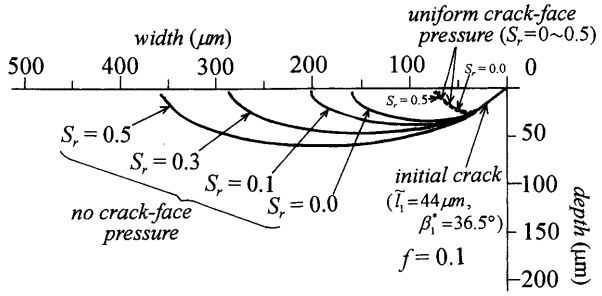

Fig. 7 Predicted of the crack path showing the thermal effect for the case of $f=0.1$

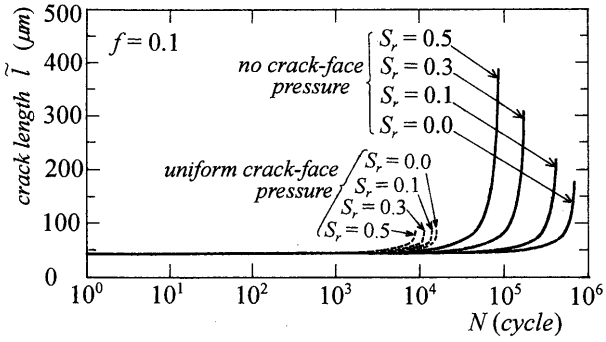

Fig. 8 Predicted crack length $\tilde{l}$ vs. cycle N showing the thermal effect for the case of $f=0.1$

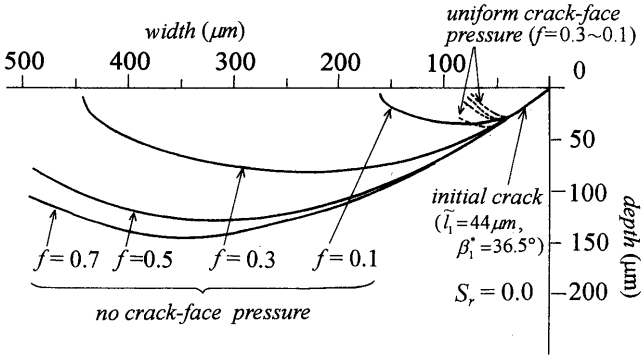

Fig. 9 Predicted crack path showing the frictional effect for the case of $S_r=0.0$

example, for the isothermal case ($S_r=0$), the fatigue life N_f decreases from a value of $N_f=6.8\times10^5$ for no crack-face pressure to a value of $N_1=1.0\times10^4$ for uniform crack-face pressure, and with an increase of thermal effect N_f decreases from a value of $N_f=1.0\times10^4$ for $S_r=0$ to a value of $N_f=7.0\times10^3$ for $S_r=0.5$.

Figure 9 displays the predicted crack growth path showing the frictional effect (f=01 - 0.7) for isothermal case ($S_r=0$). Then, the $\tilde{l}$ - N curve is shown in Fig. 10. As the frictional coefficient f increase, the fatigue life N_f is considerably reduced and a large pitting failure is formed. For example, when the crack-face pressure is absent, a maximum depth of the pit is $b=150$ μm, the fatigue life is $N_f=8\times10^3$ for $f=0.7$. The aspect ratio of the pit do not change very

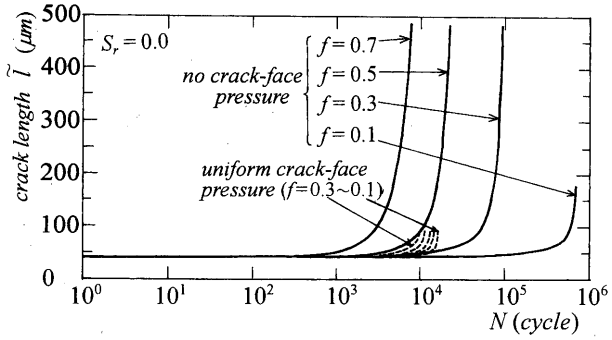

Fig. 10 Predicted crack length $\tilde{l}$ vs. cycle N showing the frictional effect for the case of $S_r=0.0$

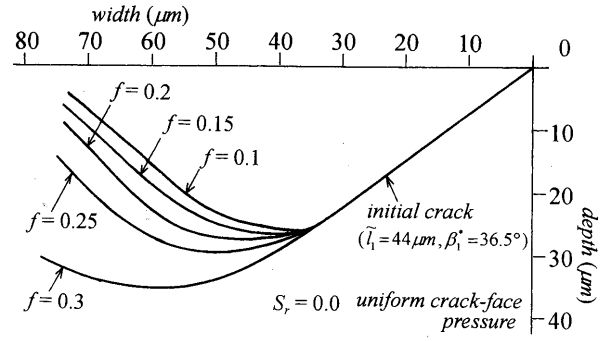

Fig. 11 Predicted crack path showing the frictional effect under the uniform crack-face pressure

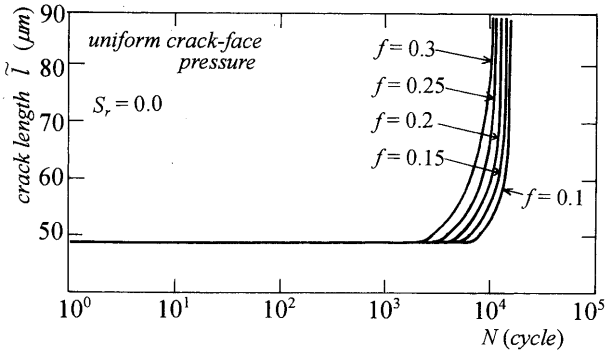

Fig. 12 Predicted crack length $\tilde{l}$ vs. cycle N showing the frictional effect under the uniform crack-face pressure

much as $b/a=0.37$ - 0.39 for $f=0.1$ - 0.7. Moreover, for the case of uniform crack face pressure, the crack growth path and the $\tilde{l}$ - N curve are display in Figs. 11 and 12 respectively. As the frictional coefficient f increase, the fatigue life N_f is reduced a little from $N_f=1.6\times10^4$ ($f=0.1$) to $N_f=1.1\times10^4$ ($f=0.3$), and a size of the pitting failure is enlarged from $b=26$ μm ($f=0.1$) to $b=35$ μm ($f=0.3$), however the aspect ratio of the pit do not change as $b/a\fallingdotseq0.65$.

Finally, in order to clarify the thermal and frictional effects on the fatigue life, Figs. 13 and 14 are the fatigue life N_f as a function of S_r for no crack face pressure and uniform crack face pressure respectively. In Fig. 13, for the case of no crack face pressure, the fatigue life N_f are shown as a function of S_r for various values of frictional coefficients: $f=0.1$, 0.3, 0.5 and 0.7. The life N_f considerably decrease with an increase of S_r. For example, for the case of $f=0.7$, with an increase of thermal effects the fatigue life is considerably reduced from $N_f=8\times10^3$ ($S_r=0$) to $N_f=6\times10^2$ ($S_r=0.5$). In Fig. 14, for the case of uniform crack face pressure, the fatigue life N_f are shown as a function of S_r for various values of frictional coefficients: $f=0.1$, 0.15, 0.2, 0.25 and 0.3. Comparing with the case of no crack face pressure (Fig. 13), we can see that uniform crack face pressure gives a much greater reduction in life due to the thermal effect. For example, for the case of $f=0.3$, with an increase of thermal effects the fatigue life is considerably reduced from $N_f=1.1\times10^4$ ($S_r=0$) to $N_f=5\times10^2$ ($S_r=0.7$).

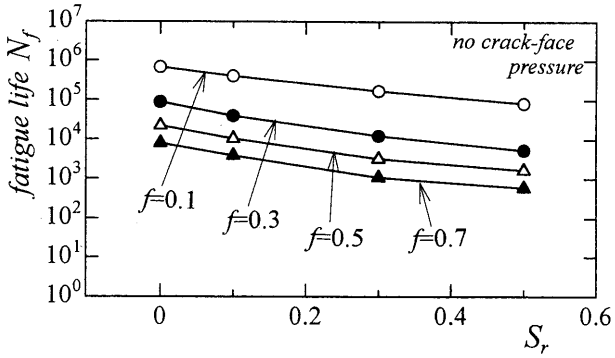

Fig. 13 Predicted fatigue life N_f as a function of S_r (thermal effect) for no crack-face pressure

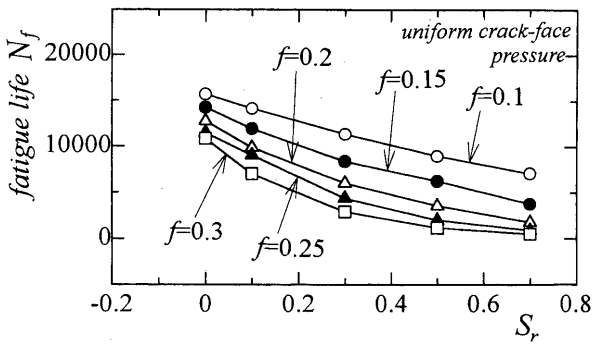

Fig. 14 Predicted fatigue life N_f as a function of S_r (thermal effect) for uniform crack-face pressure

6. Conclusions

We analyzed the stress intensity factors for a multiple kinked crack applied hydraulic internal pressure in a half-space due to rolling contact with frictional heat. From the simulation of fatigue crack growth path by applying the maximum energy release rate criterion to each kinks in order and prediction of fatigue life by making use of the fatigue crack growth

law for a high carbon chromium bearing steel (AISI52100), the following conclusions can be made.

(1) From the numerical results of stress intensity factors for the single kinked crack model, for the case of no crack face pressure or large frictional coefficient and slide-roll ratio, as $K_{I\max}$ is very small compare to ΔK_{II}, the crack propagate by shearing mode. On the other hand, for the case of uniform crack face pressure, $K_{I\max}$ become to large mixed mode propagation should be considered, and. especially, for small frictional coefficient and slide-roll ratio, $K_{I\max}$ is larger than ΔK_{II} and the crack is apt to be kinked toward to the surface with steep angle.

(2) An increase of thermal or frictional effect enlarges the size of the pitting failure, and reduces the fatigue life. Moreover, the crack-face pressure gives a much greater reduction in life and causes a smaller pitting failure as compared to no crack-face pressure.

(3) The aspect ratio of the pitting failure is almost equal to 0.65 for uniform crack face pressure and 0.33 - 0.39 for no crack face pressure. Thus, the profile of pitting failure does not change very much by the thermal and frictional effects.

References

(1) Way, S., Pitting due to Rolling Contact, Trans. ASME, J. Appl. Mech., Vol. 2 (1935), pp. 49-58.

(2) Zhou, R. S., Cheng, H. S. and Mura, T., Micropitting in Rolling and Sliding Contact under Mixed Lubrication, Trans. ASME, J. Tribol., Vol. 111 (1989), pp. 605-613.

(3) Kaneta, M., Matsuda, K., Murakami, K., Nishikawa, H. and Sugino, K., Reproduction of Rail Dark-Spot Defects, Trans. Jpn. Soc. Mech. Eng., (in Japarese), Vol. 61, No. 588, C (1995), pp. 3402-3409.

(4) Keer, L. M. and Bryant, M. D., A Pitting Model for Rolling Contact Fatigue, Trans. ASME, J. Lubr. Tech., Vol. 105 (1983), pp. 198-205.

(5) Bower, A. F., The Effects of Crack Face Friction and Trapped Fluid on Surface Initiated Rolling Contact Fatigue Cracks, Trans. ASME, J. Tribol., Vol. 110 (1988), pp. 704-711.

(6) Murakami, Y., Sakae, C., Ichimaru, K. and Morita, T., Experimental and Fracture Mechanics Study of the Pit Formation Mechanism under Repeated Lubricated Rolling-Sliding Contact: Effects of Reversal of Rotation and Change of the Driving Roller, Trans. ASME, J. Tribol., Vol. 119 (1997), pp. 788-796.

(7) Kaneta, M., Matsuda, K., Murakami, K. and Nishikawa, H., A Possible Mechanism for Rail Dark Spot Defects, Trans. ASME, J. Tribol., Vol. 120 (1998), pp. 304-309.

(8) Goshima, T. and Keer, L. M., Thermoelastic Contact between a Rolling Rigid Indenter and a Damaged Elastic Body, Trans. ASME, J. Tribol., Vol. 112 (1990), pp. 382-391.

(9) Goshima, T and Keer, L. M., Stress Intensity Factors of a Surface Crack in a Semi-infinite Body due to Rolling-Sliding Contact and Frictional Heating, Trans. Jpn. Soc. Mech. Eng., (in Japanese), Vol. 56, No. 532, A (1990), pp. 2567-2572.

(10) Goshima, T. and Ishihara, S., Fatigue Crack Growth Behavior in Cemented Carbides and Ceramics due to Repeated Rolling Contact with Thermal Stresses by Frictional Heating, Trans. Jpn. Soc. Mech. Eng., (in Japanese), Vol. 63, No. 607, A (1997), pp. 471-477.

(11) Farris, T. N., Keer, L. M. and Steele, R. K., The Effect of Service Loading on Shell Growth in Rails, J. Mech. Phys. Solids, Vol. 35, No. 6 (1987), pp. 677-700.

(12) Yu, M. M. H. and Keer, L. M., Growth of the Shell/Transverse Defect in Rails, Trans. ASME, J. Tribol., Vol. 111 (1989), pp. 684-654.

(13) Mukai, D. J., An Analysis of a Near-Surface Crack Branching under a Rigid Indenter, Trans. ASME, J. Tribol., Vol. 122 (2000), pp. 23-29.

(14) Wu, C. H., Fracture under Combined Loads by Maximum-Energy-Release-Rate Criterion, Trans. ASME, J. Appl. Mech., Vol. 45 (1978), pp. 553-558.

(15) Hanson, M. T. and Keer, L. M., An Analytical Life Prediction Model for the Crack Propagation Occurring in Contact Fatigue Failure, Trans. Tribol., Vol. 35 (1992), pp. 451-461.

(16) Dundurs, J., Mathematical Theory of Dislocations, (1975), p. 70, ASME Publication.

(17) Muskhelishvili, N. I., Some Basic Problems in the Mathematical Theory of Elasticity, 4th Ed., (1954), Noordhoff.

(18) Gerasoulis, A., The Use of Piecewise Quadratic Polynomials for the Solution of Singular Integral Equations of Cauchy Type, Comput. Math. Applics., Vol. 8 (1982), pp. 15-22.

(19) Azarkhin, A., Barber, J. R. and Rolf, R. L., Combined Thermal-Mechanical Effects in Frictional Sliding, Key Eng. Mater., Key Eng. Mater., Vol. 33 (1989), pp. 135-160.

(20) Hills, D. A. and Barber, J. R., Steady Motion of an Insulating Rigid Flat-Ended Punch Over a Thermally Conducting Half-Plane, Wear, Vol. 102 (1985), pp. 15-22.

(21) Fan, H., Keer, L. M. and Mura, T., Near Surface Crack Initiation Under Contact Fatigue, Tribol. Trans., Vol. 35, No. 1 (1992), pp. 121-127.